Optical communcation

15

Francesco Sansone
Stellar Project srl, Viale dell'Industria, Padova, Italy

15.1 Introduction

Optical communication is the exchange of information through the use of electromagnetic signals in the visible or near-infrared frequency range. Thanks to the much shorter wavelength compared to radio frequencies, very tight beams (1−100 μrad) can be realized with the use of relatively compact antennas (either reflective or refractive), which results in much higher directivity. For this reason, optical communication is an ideal technology for the realization of high throughput telecommunications with compact devices that are compatible with the small size and power that are available onboard small satellites. In addition, being the transmitted beams very tight, interception or jamming of laser links is virtually impossible, making optical communication an inherently secure technology for point-to-point communication. Besides, the application of quantum key distribution protocols over optical carriers may be used to add a further level of security to the transmission. Quantum encryption, however, is not discussed in this chapter.

The narrowness of optical beams is also the source of the main challenge related to optical communication, which is the very accurate pointing that is required to establish a communication link. In fact, the pointing accuracy of the laser beam shall be a fraction of the laser beamwidth, which is a very demanding requirement, especially if the capabilities of small satellites are considered.

The adoption of optical communication can play a key role in the augmentation of the capabilities and profitability of small satellites. On the one hand, optical communication finds an immediate use on low Earth orbit (LEO) satellites for Earth observation, allowing the downlink of data at an unprecedented rate. This will permit the full exploitation of high-resolution, multispectral imaging payloads that often can generate more data than satellites are able to download to the ground.

Optical communication may also enable intersatellite connectivity between small satellites; this functionality is currently impracticable with radio systems considering the power and mass constraints of small satellites. Intersatellite links are a key element for the implementation of satellite networks dedicated to data relay and global connectivity.

Hereafter we report a simple, yet compelling comparison between two radio-frequency downlink subsystems, one in X-band and one in Ka-band, and one optical downlink subsystem with an operational wavelength of 1550 nm, all scaled to fit

Next Generation CubeSats and SmallSats. DOI: https://doi.org/10.1016/B978-0-12-824541-5.00023-6

onboard small satellites in terms of size and power consumption. The subsystems are conceived to operate in conjunction with a ground station, whose aperture is adjusted so that the three telecom subsystems can realize downlink with the same performance. The following Table 15.1 reports the main subsystem parameters and the required aperture (both optical and radio) at the receiver station on the ground. A striking difference can be appreciated between the required aperture for the optical subsystem (<1 m) and those required for the two radio subsystems (9 and 15 m approximately). It is also noticeable the difference in required pointing accuracy for the transmit beam, which is in the order of 10 μrad for the optical subsystem and 0.5−1 degree for the radio subsystems.

Technologies for space optical communication have been developed and tested since the mid-1990s. The first optical downlink experiment was performed by NICT with the geostationary satellite ETS-VI in 1994 [1]; the first intersatellite link was demonstrated in 2003 between the ESA's GEO satellite ARTEMIS and the French LEO satellite SPOT-4 [2]; in 2006 JAXA's satellite OICETS performed the first optical downlink from LEO [3]; in 2007, the first intersatellite link between LEO satellites was carried out between the German TerraSAR-X and the US NFIRE satellite [4]; in 2013, an optical link was established from the Moon's orbit to the ground by NASA's LADEE spacecraft [5], and so on. It is worth pointing out that all the examples mentioned above were based on medium/large satellites; considering the field of small satellites, several technologies are under development aiming at compactness and low impact on the host bus, as it is described in this chapter.

The remainder of this chapter is organized as follows. Section 15.2 presents the main challenges related to optical communication systems for space applications;

Table 15.1 Comparison between transmitter subsystems for small satellites operating in X-band, Ka-band and C optical band.

Target performance	**X-band**	**Ka-band**	**Optical**
Bit rate	1 Gbps		
Bit error ratio	$\leq 10^{-5}$		
Link margin	3 dB		
Link distance	2000 km		
Transmitter section	X-band	Ka-band	Optical
Frequency	8 GHz	27.5 GHz	193 THz
Wavelength	0.037 m	0.011 m	1.55E-6 m
Transmit power	5 W	2 W	0.2 W
Transmit aperture	0.10 m	0.08 m	0.02 m
Transmit beamwidth	52.5 deg/0.92 rad	19.52 deg/0.34 rad	5.4 mdeg/95 μrad
Pointing accuracy	1 deg	0.5 deg	0.6 mdeg/10 μrad
Receiver section	X-band	Ka-band	Optical
Receive aperture	14.82 m	8.79 m	0.55 m
SNR	18.6 dB	18.6 dB	19.4 dB

Section 15.3 provides an analytical tool for the evaluation of the link budget; Section 15.4 describes the most common modulation techniques used in free-space optical communication (FSOC); Section 15.5 presents the main options for optical communication terminal architecture; Section 15.6 provides an overview of the existing or under development optical communication terminal suitable for small satellites; finally, conclusions are given in Section 15.7.

15.2 Challenges of optical communications

15.2.1 Pointing, acquisition and tracking

In order to establish a stable optical link, the communicating terminals must achieve a line of sight (LoS). The uncertainty cone, that is, the uncertainty on the LOS direction in the satellite reference frame, is typically larger than the transmit laser beamwidth. The main contributors to the uncertainty cone are the uncertainty on the satellite ephemeris, the attitude determination and control subsystem (ADCS) accuracy and the mechanical/optical misalignments between the laser communication terminal and the host satellite bus; they are summarized in Table 15.2. Considering laser wavelengths between 800 and 1550 nm, which are commonly used, and an optical aperture of 50 mm, transmit laser beamwidth is 20−50 μrad. Required pointing accuracy for optical communication is a fraction (rule of thumb: one-fifth) of the laser beam divergence in order to minimize losses, which results in 4−10 μrad, which is beyond the typical performance of ADCSs of small satellites, and especially nanosatellites. Thus, precise pointing is achieved by tracking a beacon laser that is transmitted by the partner satellite (in case of intersatellite links) or from a ground station (in case of downlink), with the use of dedicated pointing systems (gimbals, tip/tilt mirrors, or combination of both).

Mutual tracking is required in order to correctly transmit and receive over an optical channel. Very often, the transmit laser beamwidth is smaller than the uncertainty cone and so an acquisition procedure must be performed, during which the two terminals point toward each other in an open loop based on the predicted orbital positions of the satellites. Then, each terminal scans its beacon beam over the uncertainty cone, until the beam is detected by the partner terminal which can lock on it and start tracking. This acquisition phase is complete when both terminals have acquired and are tracking the beacon beam sent by the partner terminal.

Table 15.2 Main contributors to uncertainty cone.

Uncertainty cone contributor	Value (degrees)
Ephemeris uncertainty	0.05
ADCS accuracy	0.20
Misalignments	0.10
Total	0.23

In some cases, acquisition phase can be avoided, at least on one side, if the beacon laser divergence is larger than the uncertainty cone. The most common case is when one of the terminals is an optical ground station in a LEO downlink scenario; in this case, there are no particular constraints on the power available to the beacon laser, whose beam divergence can be widened in order to cover the whole uncertainty cone. The main contribution to the latter, in this case, is the uncertainty on the satellite position given by orbital propagation (from two-line element or global navigation satellite system data). Typically, a full beam divergence in the 0.6−1 mrad range is sufficient to cover the whole cone of uncertainty [6,7]. The output power shall be set accordingly, taking into account the minimum power that is required by the flight terminal sensor to close the acquisition loop.

Finally, the finite velocity of light must be considered for the precise pointing of the transmit laser beam. In fact, an offset angle between the received beacon/telecom beam and transmitted beacon/telecom beam must be introduced to take into account the relative motion between the terminals in the time interval required by photons to travel from one terminal to the other. This angle is called the point-ahead angle and can be easily calculated as

$$\alpha = \frac{2V_r}{c} \tag{15.1}$$

where c is the speed of light and V_r is the component of the relative velocity of the two terminals orthogonal to the LoS. Depending on the orbit, the point-ahead angle may be comparable to the transmit laser beamwidth and may require a dedicated pointing system (see Section 15.5).

15.2.2 Optical output power

Another critical point is represented by the optical output power that is required to achieve a signal-to-noise ratio at the receiver that can guarantee bit error rate values that are acceptable (typically desired uncoded BER is $<10^{-5}$). Different strategies are adopted in order to maximize the optical output power of the modulated laser beam.

One common solution envisages the use of a low-power (≈ 1 mW) laser source that generates a modulated optical signal by means of direct modulation of its feed current. The modulated signal is then amplified by the use of an optical amplifier, which is typically available for wavelengths of 980 nm, 1064 nm (Ytterbium Doped Fiber Amplifier), 1550 nm (Erbium Doped Fiber Amplifier), with amplification gain in the order of 20 dB. This solution allows for high modulation bandwidth (up to a few Gbps), with output power in the order of 2 W. The use of a low-power laser source simplifies the thermal management of the system. However, optical amplifiers are generally low power-efficient and their use comes at the cost of increased complexity, size and power consumption.

An alternative solution is the use of a medium-high power laser source (hundreds of mW) whose optical carrier is then modulated by the use of an optical modulator.

Here the bottleneck is represented by the maximum input power accepted by optical modulators, which is typically in the order of few hundreds of mW, with maximum values of 300 mW.

15.2.3 Atmospheric effects

In satellite-to-ground optical links, the crossing of the atmospheric layers plays a crucial role in the free-space propagation of the laser beam, resulting in a different types of phenomena that affect the overall link performance. Such phenomena are due to atmospheric absorption, scattering and turbulence, which are briefly described in the following paragraphs.

15.2.3.1 Atmospheric absorption and scattering

In clear sky conditions, the power losses that a propagating laser beam is subjected to are due to absorption and scattering of light, which are caused by the interaction between the laser beam and molecules, aerosol and larger particles in the atmosphere.

Absorption in the visible and near-infrared spectrum is due to aerosol and molecules of water, ozone and carbon dioxide, and is a wavelength-dependent phenomenon. There exist wavelength windows that are less affected by absorption and are typically exploited for FSOC, especially in the 780−850 nm and 1520−1600 nm intervals. Typical values of molecular absorption in dB/km for common laser wavelengths are reported in Table 15.3 [8].

Light scattering also depends on the laser wavelength. If the size of atmospheric particles is smaller than the wavelength, then Rayleigh scattering occurs. This phenomenon is more evident for visible and ultraviolet lasers and is due to air molecules and haze. If instead, the size of atmospheric particles is comparable with or larger than the wavelength, Mie scattering is produced, which is due to aerosol particles, dust, fog and haze. Mie scattering is prominent for near-infrared lasers.

Channel attenuation due to absorption and scattering can be modeled with Beer's law [9], which gives the atmospheric losses L_a in [dB] (see also link budget in Section 15.3) as a function of the propagation distance d [km] and the absorption and scattering coefficients α_a and α_s [km^{-1}], which are wavelength-dependent.

Table 15.3 Values of molecular absorption for laser wavelengths typically used for FSO [8].

Wavelength (nm)	Absorption (dB/km)
550	0.13
690	0.01
850	0.41
1550	0.01

Their values can be found in available databases [10]. Their sum α_e is referred to as *extinction coefficient*.

$$L_a = e^{-\alpha_e d} \tag{15.2}$$

$$\alpha_e = \alpha_a + \alpha_s \tag{15.3}$$

In clear sky conditions, L_a is in the order of -1 to -3 dB, depending on the laser wavelength and with lower values for higher wavelengths. In adverse weather conditions (cloud, rain, fog), the power attenuation L_a can be of tens or hundreds of dB, making optical links impossible.

A more detailed description of absorption and scattering loss can be found in [8,11].

15.2.3.2 Atmospheric turbulence

Random variations in the atmospheric temperature and pressure along the laser path cause the formation of turbulent cells that cause constructive or destructive interference of the propagating beam. This is called atmospheric turbulence. Three types of effects can be described, which depend on the size of the turbulent cells compared to the beam size.

When the turbulence cells are larger than the beam size, beam wandering occurs. This is a random deflection of the propagating beam and it is particularly evident for ground uplink beams. In fact, they cross the atmosphere at the beginning of their propagation path, where the beam has not expanded much yet. Beam wandering displacement is described in [12].

When the turbulence cells are smaller than the beam size, distortion of the received wavefront occurs.

When the turbulence cells are comparable with the beam size, scintillation occurs. This phenomenon consists of fluctuations in the intensity of the received beam and is a major cause of performance degradation in downlink (or air-to-air) optical channels. Scintillation is expressed in terms of the scintillation index, which is described in [13,14].

Atmospheric turbulence is a wide and complex topic that cannot be discussed in detail in this chapter; nevertheless, a comprehensive description of atmospheric turbulence and its effects on FSOC can be found in the literature [15].

15.3 Link budget

As it is common for radio-based telecommunication systems, a link budget is used to numerically evaluate the performance of optical communication. Link budget is based on the power budget that is described by Eq. (15.4), which relates the received optical power P_{RX} to the transmitted optical power P_{TX}, the gains of the

transmit optics G_{TX} and the gain of the receive optics G_{RX}, and the losses that occur on the optical channel, which are the pointing loss L_P, the free-space loss L_S due to light propagation, the line loss L_L due to the efficiency of the optical elements and the atmospheric loss L_A due to absorption of the atmosphere (in satellite-to-ground scenarios). The main parameters of the power budget are calculated accordingly to the following equations, where β is the transmit beam full divergence ($1/e^2$, assuming Gaussian power distribution for the laser beam), D_{RX} is the receiver aperture diameter, ε is the pointing error and L is the link distance. The laser beamwidth β is defined as double the angular width for which the intensity of the radiation falls from maximum to a given value; the latter can be set to zero (thus corresponding to the Airy disc radius, used in classical optics to describe a plane wavefront illuminating an aperture homogeneously) or to half of the maximum power. In general, β is a function of the illuminated aperture D_{TX} and the laser wavelength and, considering diffraction-limited optics, can be approximated by Eq. (15.9), where $k = 1.22$ if the Airy disc radius criterion is applied or 1.03 if the half-power criterion is applied.

$$P_{RX} = P_{TX} G_{TX} L_L L_P L_S L_A G_{RX} \tag{15.4}$$

$$G_{TX} = \frac{16}{\beta^2} \tag{15.5}$$

$$G_{RX} = \left(\frac{\pi D_{RX}}{\lambda}\right)^2 \tag{15.6}$$

$$L_P = -8.7\left(\frac{2\varepsilon}{\beta}\right)^2 \tag{15.7}$$

$$L_S = \left(\frac{\lambda}{4\pi L}\right)^2 \tag{15.8}$$

$$\beta = k\frac{\lambda}{D_{TX}} \quad k = 1.22(\text{Airy disc}), k = 1.03(\text{half power}) \tag{15.9}$$

L_L is very dependent of the layout and technical solutions adopted for the optical terminals and L_A depends on the weather: it ranges from as low as -1 or -2 dB in case of clear sky up to a few tens of dB in case of rain and/or cloud coverage, which results in the impossibility to close the power budget.

Link budget is then completed by the calculation of the signal-to-noise ratio at the receiver, which ultimately is related to the bit error ratio. The SNR depends on the characteristics of the receiver, which is usually a photodiode whose photocurrent is electrically amplified (e.g., by a transimpedance amplifier). By definition

$$\text{SNR} = \frac{P_{\text{signal}}}{P_{\text{noise}}} \tag{15.10}$$

P_{signal} is the power of the electrical signal [W] generated by the conversion of the optical photons to electrical current by the receiver detector and is proportional to the square of the photocurrent I_{PH}, which can be expressed as

$$I_{PH} = rP_{RX} \tag{15.11}$$

where r is the detector responsivity (A/W). The noise power [W] is given by the shot noise contribution P_{sh} and the thermal noise contribution P_{th}, as described by Eqs. (15.9) and (15.10), where q is the elementary charge, Δf is the receiver bandwidth, I_d is the photodiode dark current, k_B is the Stefan-Boltzmann constant, R_L is the load resistor, T is the load resistor temperature, F_N is the noise figure of the electrical amplifier.

$$P_{\text{sh}} = 2q\left(I_{ph} + I_d\right)\Delta f = 2q(rP_{RX} + I_d)\Delta f \tag{15.12}$$

$$P_{\text{th}} = \frac{4k_B T}{R_L} F_N \Delta f \tag{15.13}$$

$$\text{SNR} = \frac{r^2 P_{RX}^2}{2q(rP_{RX} + I_d)\Delta f + \frac{4k_B T}{R_L} F_N \Delta \text{f}} \tag{15.14}$$

In case the thermal noise is dominant ($P_{\text{th}} >> P_{\text{sh}}$), the SNR becomes:

$$\text{SNR} = \frac{r^2 P_{RX}^2 R_L}{4k_B T F_N \Delta \text{f}} \tag{15.15}$$

In this case, noise can be represented by the noise-equivalent power (NEP), defined as the minimum optical power per unit bandwidth required to produce SNR = 1 [see Eq. (15.16)].

$$\text{NEP} = \frac{P_{RX}}{\sqrt{\Delta \text{f}}} = \left(\frac{4k_B T F_N}{r^2 R_L}\right) \tag{15.16}$$

The NEP is often used to describe the performance of optical detectors and is typically available on the detector datasheets. Optical power needed to realize a specific value of SNR is obtained from Eq. (15.17).

$$P_{\text{min}} = \text{SNR}\text{NEP}\sqrt{\Delta f} \tag{15.17}$$

The SNR define the channel capacity C, that is, the maximum achievable data rate R_{max} with a given BER, applying the maximum possible efficiency of error-correcting coding [16], see Eq. (15.18). The latter can be re-arranged as Eq. (15.19), where E_b is the energy per bit, N_0 is the noise spectral density and

P_{noise} is defined as $N_0\ \Delta f$. E_b/N_0 is called power efficiency and $R/\Delta f$ is called bandwidth efficiency. Eq. (15.19) describes the condition required for possible error-free communication. For a given SNR, applied data rate shall satisfy these conditions in order to have error-free communication.

$$C = R_{\max} = \Delta \text{f} \log_2(1 + \text{SNR}) \tag{15.18}$$

$$\frac{E_b}{N_0} > \frac{2^{R/\Delta \text{f}} - 1}{R/\Delta \text{f}} \tag{15.19}$$

15.4 Modulation

Modulation of optical signals can occur in different ways and methods. Modulation can change the intensity of the transmitted laser (amplitude modulation) or change the phase of the carrier wave. Also, detection can be direct, that is, only the transmitted signal is detected by the receiver, or coherent, which means the receiver detects not only the transmitted signals but also a reference signal generated locally, whose wavelength and modulation frequency match those of the transmitted signal. An exhaustive overview of modulation techniques can be found in [17]; hereafter, we briefly introduce the most common ones used in FSOC.

The simplest form of modulation is on-off keying (OOK), which is a binary intensity modulation of the transmitter laser. Ideally, peak power corresponds to "1" and zero power (laser turned off) corresponds to "0"; in practice, the laser may not be turned off but simply regulated at a minimum level to encode the "0," especially if high modulation frequencies are sought. OOK is a direct detection modulation. Its main advantage is the simplicity and low cost of hardware, making it a suitable solution for small satellites in LEO-to-ground applications. However, it has relatively low spectral and energy efficiency. In fact, being T the repetition rate of the pulses of peak power Pp, the maximum bitrate is $1/T$ and the average power is 0.5 Pp.

An improved version of OOK is pulse position modulation (PPM); the time slot T allocated for each bit is divided into M slots; the position of the impulse of duration T/M in one of the M slots encodes one of the 2 M possible values. This way, peak power is increased by reduction of the laser duty cycle while keeping the same average power of the OOK modulation; the resulting bit rate is M/T and peak power is M Pp. Thus, PPM has higher energy efficiency than OOK but lower spectral efficiency since a higher modulation frequency is required, which may limit the application of high-order PPM on small satellites. PPM is suitable for energy-constrained systems or when photon-counting receivers are used; the latter are hardly applicable on small satellites due to hardware complexity, thus PPM is more suitable for LEO-to-ground applications.

Another direct detection modulation technique is phase-shift keying, which consists to assign to each bit a given carrier phase. In its simplest version (binary phase-shift keying, BPSK), two-phase levels are used, respectively 0 and 180 degrees, encoding "1" and "0." This is the most noise-insensitive form of PSK but also the less efficient (1 bit/symbol). Higher order schemes, such as quadrature PSK, encodes more symbols per bit using more phase-shift values (0, 90, 180, and 270 degrees for QPSK, corresponding to "00," "01," "10," "11"). M-ary PSK encodes M bit/symbol. The spectral efficiency in [bps/Hz] of MPSK is given by Eq. (15.20).

$$e = \frac{\log_2 M}{2} \tag{15.20}$$

A modified version of PSK is differential phase-shift keying (DPSK), which consists in shifting the carrier wave phase from its last position by a given amount, based on the bit (1 or 0) to be transmitted. For example, in binary DPSK (DBPSK) the shift is 180 degrees for "1" and 0 degree for "0," while in DQPSK the phase shifts are 0, 90, 180, −90 degrees corresponding to data "0," "01," "11," "10." DPSK overcomes one issue affecting PSK, which is the possible ambiguity of phase in case of arbitrary phase shift introduced by the communications channel through which the signal passes.

Compared to OOK and PPM, PSK is less sensitive to background noise since the latter mostly affects the intensity of the signal rather than its phase. For this reason, DPSK is a good choice for atmospheric FSOC.

Coherent detection and demodulation consist in mixing the received signal with a locally generated oscillator that matches the received signal's optical wavelength, frequency and phase. Both signals are sent to the optical receiver; the mix of the high-power local oscillator and the modulated low-power received signal generates an amplified signal that keeps the modulation of the original received signal and has intensity well above the noise level of the receiver electronics. Background noise rejection is improved with respect to direct detection, resulting in higher SNR and improved detector sensitivity. For these reasons, coherent detection is used in intersatellite links over long distances (e.g., LEO-GEO).

15.5 Optical terminal architecture

Optical communication terminals can be based on different architectures and exploit different technical solutions. A broad distinction can be made between monostatic and bistatic systems.

In monostatic systems, the transmit and receive beams pass through the same optical antenna (refractive, reflective or a mix of both) and share most of the optical patch. Monostatic design is typically more compact and is simpler in what concerns the pointing system control; however, the complexity of the optical system needed

to manage the routing of the transmit and receive signals on the same optical path is higher.

On the other hand, bistatic systems have distinct apertures and optical paths for transmit and receive beams; this also implies distinct fine-pointing systems (FPSs). Instead, the coarse pointing system (CPS) is usually one for both beams (this may be represented by a gimbal or, in case of small satellites, by the host satellite platform). Bistatic systems feature simpler optical systems but the duplication of optical paths and FPSs results in bulkier and more power-consuming systems. The layout of monostatic and bistatic systems are shown in Fig. 15.1

Despite the diversity of architectural solutions, some key building blocks are common to all terminals. In Fig. 15.2, a functional scheme of the typical optical communication terminal is presented. Blue blocks are common to all architectures, green blocks are optional. Two units are identified, namely the electronic unit (ELU), which contains the laser source(s), the detectors required for pointing and for telecommunication reception, and their conditioning electronics, and the opto-mechanical unit (OMU), featuring the pointing system, the telescope and the focal plane. The system presented in Fig. 15.2 is monostatic for what concerns the telecommunication beams but features a bistatic solution for the beacon laser.

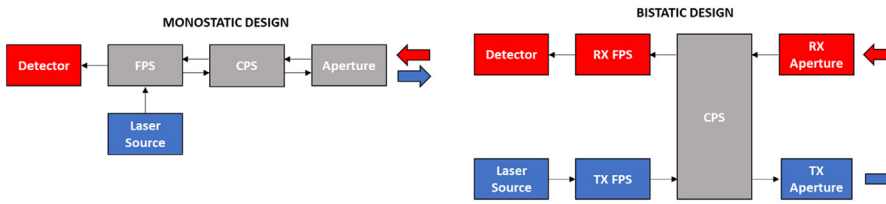

Figure 15.1 Monostatic (left) versus bistatic (right) architecture for laser communication terminals.

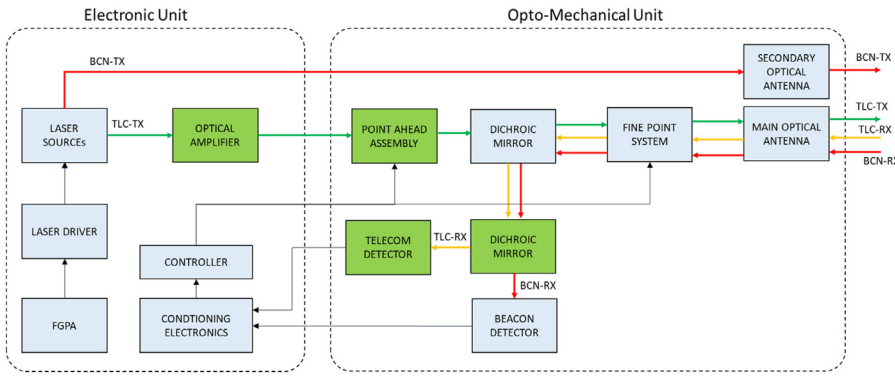

Figure 15.2 Architecture of optical communication terminals.

The OMU features the main optical antenna that is used to collimate the transmit beam and to collect and focus the received beams on a detector. At least one received beacon beam is needed to provide a feedback signal that is used for pointing the optical antenna and for fine alignment corrections performed by the fine point system.

The transmit beacon laser can share the same optical path as the received beacon laser or it can be routed to a secondary antenna via a secondary path; the main reason behind the second solution is to avoid back reflections that can blind the beacon detector if transmit and receive beacon lasers have the same wavelength (in fact, power of transmit and receive signals may be orders of magnitude apart).

Pointing of the optical antenna can be performed by a dedicated mechanical system or can be carried out by the satellite bus. A dichroic mirror is used to separate the optical path of the transmit and received beacon beam, based on wavelength separation. The same can be applied in the case a telecom beam is also received if its carrier has a different wavelength than the transmit one's. Different solutions may be adopted as beacon detectors; the most common are quadrant detectors (or avalanche photodiode quadrant detectors for enhanced responsivity) or focal plane arrays (i.e., CCDs or CMOS sensitive to optical and near-infrared wavelengths). QDs are characterized by high bandwidth (up to MHz), which makes them suitable for high-bandwidth pointing control systems; this is because the information of the laser spot position on the sensitive area can be readily calculated from the four channels output voltages by simple geometrical relations. Instead, FPA requires image processing for the extraction of the laser spot position on the detector-sensitive area, with typical bandwidth limited to a few tens Hz. However, they can provide a larger field of view (FoV) with respect to QDs, which work better for centering applications since the focused laser spot shall illuminate all four quadrants.

As an alternative, position-sensitive devices can be used; they are composed of a single photodiode cell with a relatively large area (up to 10−20 mm) and their logic is similar to that of quadrant detectors. Their downside is relatively low sensitivity.

The point ahead assembly is optional since it is required only if the transmit laser beamwidth is comparable to the point ahead angle; on the contrary, if the point ahead angle is much smaller than the transmit beamwidth, an active point ahead may be avoided and the pointing error introduced by the point-ahead angle can be treated as an additional pointing loss. Finally, optical amplifiers may be used to increase the optical output power of the transmit laser. This is a typical solution when the laser source is a low power (few mW) and it is directly modulated through modulation of its feed current by the driver, which is commanded by an FPGA.

15.6 Optical communication terminals for small satellites

This section provides an overview of existing and under-development optical communication terminals for small satellites. At the end of the section, a quantitative comparison of the presented terminals is given through performance charts.

15.6.1 Small optical transponder

The Small Optical Transponder (SOTA) is a miniature lasercom terminal developed by the Japanese National Institute of Information and Communication Technology (NICT) [18]. SOTA was the main scientific payload of the satellite Space Optical Communications Research Advanced Technology Satellite (SOCRATES), launched in May 2014. The mission demonstrated optical downlink at 10 Mbps and the first quantum-communication experiment from space, receiving information from the satellite in a single-photon regime by an optical ground station [19].

SOTA is composed by an OMU (SOTA-OPT) and an ELU (SOTA-CONT), which are shown in Fig. 15.3. Total mass is 5.7 kg (2.5 for SOTA-OPT, 2.8 for SOTA-CONT and 0.4 for SOTA-WHN).

SOTA-OPT features a coarse pointing mechanism based on a 2-axis gimbal system to orient the optical head. The gimbal is actuated by stepper motors with Harmonic Drive reductors, with a reduction ratio of 1:100. The operational range is +/− 45 degrees on each axis, with a maximum angular velocity of 3 degrees/second. Resolution is 0.001125 degree/pulse and backrush of 20 arcsec. The optical head contains a lightweight Cassegrain telescope with a 50-mm diameter, which is used as an optical antenna for receiving beacon and telecom signals from the ground. The received beacon signals are focused on a quadrant detector; the latter serves a fine pointing mirror used to center received telecom signals at 1064 nm on a multimode fiber connected to a PIN photodiode in SOTA-CONT and to correctly point the transmitted signals at 1543 nm. The optical head also features an external quadrant detector with an aperture of 23 mm, used for acquisition and tracking purposes. The system features four laser transmitters in total, named TX1 to TX4; TX1 operates at 980 nm, TX2 and TX3 at 800 nm and TX4, which is embedded in the optical antenna assembly, operates at 1543 nm. TX2 and TX 3 are used for basic quantum measurements for satellite quantum key distribution and their light is linearly polarized, while TX1 and

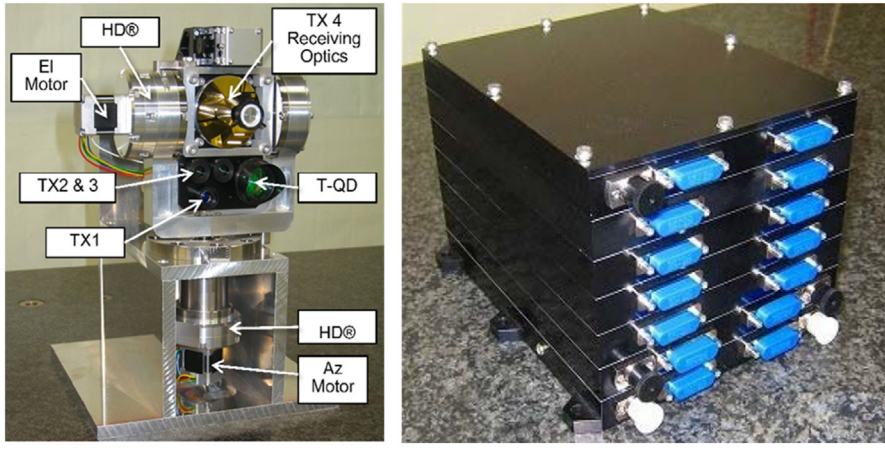

Figure 15.3 Left: SOTA-OPT PFM; right: SOTA-CONT PFM [21].

TX4 are used for data transmission. Power output of TX1 and TX4 is 540 and 80 mW, respectively. Transmitted beam divergence is 0.5 and 0.2 mrad, respectively. The maximum achievable data rate is 10 Mbps. Total power consumption is 28 W operating TX4 and 39.5 W operating TX1. Volume is $177.5 \times 117 \times 278$ for SOTA-OPT and $146 \times 160 \times 110.5$ for SOTA-CONT.

NICT have developed a smaller version of the SOTA system, called VSOTA (Very Small Optical Transponder) [20]. This device is conceived to operate onboard RISESAT, which is a 50 kg, $50 \times 50 \times 50$ cm^3 microsatellite launched in January 2019. Due to mass and volume constraints, VSOTA lacks a gimbal system for coarse pointing, thus it relies on its host satellite attitude control system for that operation. The maximum mass and total power consumption of VSOTA are 1 kg and 10 W; the system, which is transmit-only, uses two different lasers, TX1 and TX4, operating at 980 and 1550 nm, with an emitted output power of 540 and 80 mW; their beam divergence is 3.5 and 1.3 mrad, respectively. The foreseen data rate is between 1 and 100 kbps over a maximum distance of 2000 km. The system is composed of two main parts: VSOTA-COL, which contains the optical elements and is mounted on the face of RISESAT facing the Earth, and VSOTA-E, which contains the control unit of the transmitter laser diodes.

15.6.2 OCSD

In the framework of the NASA Optical Communications and Sensors Demonstration (OCSD) program carried out by the Aerospace Corporation, a compact laser transmitter terminal has been developed and tested [22,23]. The technology demonstration mission exploited two twin 1.5 CubeSats, AC-7B&C, launched in 2017 in 450 km circular orbit, each one equipped with a lasercom transmitter and an attitude control system dedicated to provide the pointing accuracy required to establish optical downlink toward a 40-cm ground telescope. In fact, the OCSD lasercom terminal is not provided with a dedicated CPS but rather it exploits the ADCS of the host platform.

The OCSD spacecraft ADCS exploits sun and Earth nadir sensors for coarse attitude determination, while for fine attitude determination to be used during laser pointing two alternatives are available. The main option is the use of star trackers; the secondary approach implements an uplink ground laser beacon (5 W at 1550 nm) and onboard quadrant detector for closed-loop pointing. Both methods are expected to provide better than 0.015 degree of attitude knowledge, while heritage 3-axis reaction wheels will provide a 0.015 degree pointing accuracy. A triad of torquerods complements the ACS system.

The lasercom terminal consists in a two-stage laser emitter, whose architecture is reported in Fig. 15.4 left. A low-power distributed feedback 1064 nm laser is directly modulated (current modulation) to implement OOK encoding; the modulated signal is amplified from 10 mW to 2−4 W by a single-stage polarization-maintaining ytterbium-doped fiber amplifier. The divergences of the output laser beams for AC-7B and AC-7C were set to be 0.06 and 0.15 degree FWHM, respectively. Such conservative values were chosen in order to be at least twice the expected pointing accuracy.

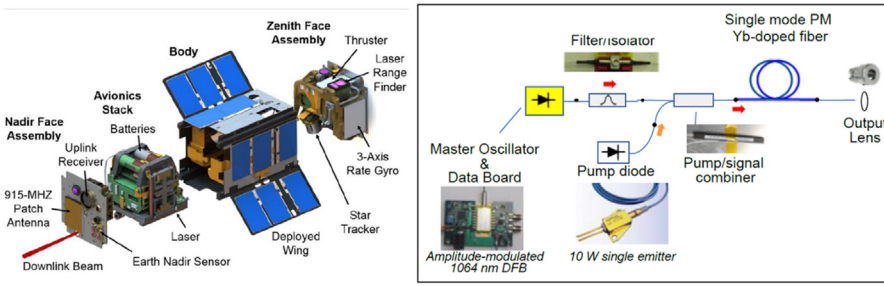

Figure 15.4 (Left) Breakout of AC-7B&C spacecraft. (Right) Schematic drawing of the OCSD laser downlink transmitter [22].

The laser transmitter volume is roughly $100 \times 100 \times 25$ mm.

Optical downlink experiments have been carried out with a 40 cm aperture, 3 m focal length Ritchey−Chrétien ground telescope, at elevation angles between 30 and 70 degrees. Data were collected at 50 and 100 Mbps. In the first case, BERs near 1E-6 and below were observed with numerous intervals being error-free. At 100 Mbps, BERs approaching 1E-6 was also observed, but with no error-free intervals.

Power consumption can rise up to 22 W during downlink operations due to the amplifier pump lasers; heat is transferred to the aluminum body of the spacecraft which acts as a temporary heatsink.

15.6.3 Nanosatellite optical downlink experiment and Cubesat laser infrared crosslink

The Nanosatellite Optical Downlink Experiment (NODE) developed by MIT is a transmit-only laser communication terminal conceived for nanosatellites based on the CubaSat standard; it is designed to fit in platforms starting from the 3U size [24,25]. The system fits in 1.2U, has a mass of 1.2 kg and power consumption of 15 W. The transmitter section consists of a low-power 1550 nm laser source and an erbium-doped fiber amplifier (EDFA) that rises the optical output power to 0.2 W. Transmitted beam has a half-power beamwidth of 1.3 mrad; M-ary PPM is applied to the transmitted laser carrier to support rate-scalable data transmission (e.g., rates greater than 40 Mbps to a 1 m terminal or 10 Mbps to a 30-cm terminal).

The pointing system of NODE is based on a MEMS fast steering mirror that is used for fine pointing of the transmit laser beam; to close the control loop, a beacon signal at 976 nm sent by the ground station is detected by a 5-degree field-of-view CMOS camera. Coarse pointing is provided by the host satellite ADCS; the NODE payload pointing system supports bus pointing errors within $+/-3$ degrees open-loop and is limited by the beacon camera field-of-view. For the host bus to track the ground station, slew rates of up to 1.1 degree/second must be supported for LEO satellites at 400 km, while lower slew rates are required for higher orbits. The NODE pointing, acquisition and tracking (PAT) system has been validated in the laboratory against a simulated bus coarse pointing error of $\pm$ 0.15 degree (3σ)

with the stability of ± 0.0225 degree/second (3σ) and maximum pointing bias of ± 1 degree. In such conditions, the NODE PAT system showed a total tracking error of 20 μrad with a standard deviation of 10.5 μrad.

Stemming from the experience of NODE, an augmented terminal for intersatellite optical communication has been developed by MIT, to be tested with the proposed Cubesat Laser Infrared CrosslinK (CLICK) B/C mission [26]. This mission comprises two 3U CubeSats, equipped with identical lasercom terminals. The CLICK terminal fits in 1.5U and has a mass of 1.7 kg and is conceived to operate in conjunction with a twin unit on another satellite for reciprocal tracking and bidirectional communication. For this reason, new with respect to the NODE terminal is the inclusion of a telecom receiver channel and a beacon laser transmitter to be tracked by the twin terminal for fine pointing purposes; the coarse pointing is still delegated to the host spacecraft ADCS. The mission goal is the demonstration of 20 Mbps over a 580 km link distance.

Transmit laser has a wavelength of 1563 nm (CLICK A) and 1537 nm (CLICK B), output power of 0.2 W and beam divergence of 121 μrad ($1/e^2$). Beacon laser works at 975 nm, has output power of 250 mW and a divergence of 7.147 μrad ($1/e^2$). Receiver aperture is 23 mm. In addition to the NODE camera, a quad-cell detector is added to improve beacon laser tracking accuracy.

15.6.4 Fibertek laser communication terminal

Fibertek has developed a generation 1 laser communication terminal (LCT) that fits in 2 CubeSat units [27]. It is composed of the lasercom optics module (LOM) and the lasercom electronics module (LEM), as shown in Fig. 15.5.

The LOM contains a 64-mm reflective off-axis telescope which is used as a common transmit and receive aperture. The monolithic optical assembly includes the bulk transmit and receive aft optics.

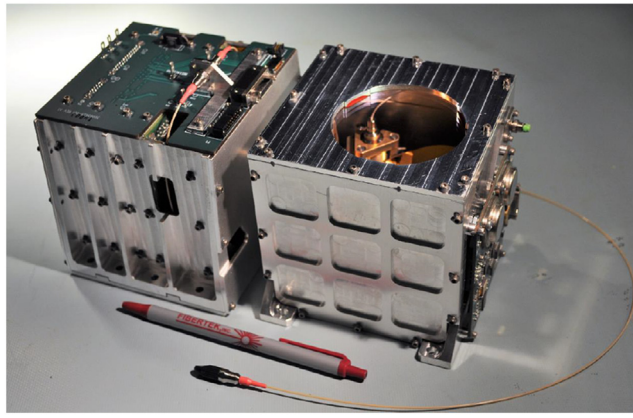

Figure 15.5 Fibertek lasercom terminal consisting of electronics module (left) and optical module (right), each one fitting in 1 CubeSat unit [27].

The LOM module also includes the fast-steering mirror and beacon position sensing detector board for precision pointing and point-ahead capability. The beacon sensor is upgraded for higher sensitivity and compatibility with a 1.5-μm beacon. For near-earth applications, a position-sensing detector is used. For longer-range applications, the position-sensing detector is replaced with a focal plane array for extended sensitivity and deep-space communications.

The LEM consists of the power distribution unit (PDU), RF modem with optical transceiver, EDFA and a system controller. The PDU supports 12 or 28 V unregulated bus supply and provides power to all LEM and LOM subsystems. The modem has a Gigabit Ethernet (GbE) client interface, FPGA-based encoding/decoding and an optical transceiver for the FSO interface. The modem supports OOK, PPM, and in the future, DPSK. The radiation-tolerant EDFA provides up to 3 W output transmit power to support extended ranges and data rates. The radiation-tolerant FPGA-based system controller interfaces with the host through RS-485 communications for control and telemetry data. The system controller also handles the fast acquisition, fine-pointing and point-ahead correction in conjunction with the fine-steering mirror and beacon sensor on the LOM module. The LEM and LOM modules weigh about 1 kg each for a total system weight of about 2 kg. Power consumption is 20 W.

15.6.5 LaserCube

LaserCube is an optical communications terminal developed by Stellar Project and conceived as a high-throughput telecom subsystem for micro and small satellites [28]. The system is composed of the OMU and the ELU, which are shown in Fig. 15.6. Mass, power and volume are <2 kg, $<$ 26 W, and 2.2 U, of which, the OMU fits in 1U and the ELU in 1.2U.

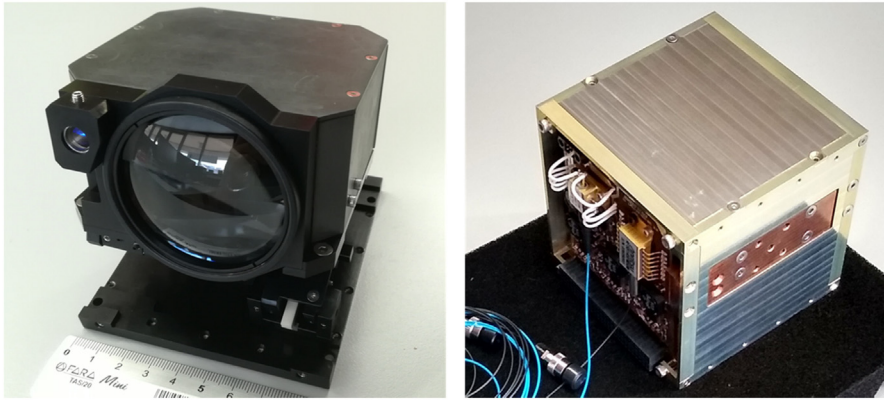

Figure 15.6 LaserCube downlink terminal. (Left) OMU; (right) electronic unit [31]. *OMU*, Optomechanical unit.

The OMU is provided with a dual-stage pointing system, which is composed of an innovative CPS based on the parallel platform configuration, patented by Stellar Project, and a fast-steering mirror present in the optical head. The coarse pointing mechanism has a $+/-10$ degrees range on elevation and azimuth and accuracy in the order of 60 μrad, when operating in a closed loop in conjunction with a ground laser beacon and a quadrant detector present in the optical unit, which is directly mounted on the CPS. The optical unit features a 42-mm optical aperture, a fast-steering mirror for fine pointing, a dichroic mirror used to separate telecom and received beacon signals and a quadrant detector providing pointing error feedback to the dual-stage pointing system. The carrier wavelength is 1550 nm both in transmission and reception; each unit is also provided with a second laser source for pointing purposes (900 nm or 1064 nm).

The dual-stage pointing system demonstrated pointing accuracy better than 10 μrad rms [29,30].

The ELU contains the Power Conversion and Distribution Unit, the Payload Control and Conditioning Unit, the Telecom Management Unit, the Actuator Driver Unit and the Laser Driver Unit. The electrical interface features nominal and redundant connectors for power and TM/TC; the accepted input voltage is 16−40 V. Communication with the host satellite is performed through Can Bus.

The terminal comes in two possible configurations that are optimized for downlink and intersatellite link, respectively. LaserCube-Downlink can transmit up to 2 Gbps from LEO to the ground using an optical modulator to impose modulation of the telecom laser carrier at GHz frequencies [31]. LaserCube-ISL units can exchange data at up to 100 Mbps over 1000 km. In this case, direct modulation of the laser current is applied.

LaserCube-Downlink was launched onboard D-Orbit's ION-SCV 003 Dauntless David satellite in July 2021.

15.6.6 Optical space infrared downlink system program

In the framework of the DLR's Optical Space InfraRed downlInk System (OSIRIS) program, four generations of compact optical terminals for LEO downlink applications have been developed in the last few years.

OSIRIS V1 is the first terminal of this program and consists of a laser transmit unit and a dedicated power supply unit [32]. The terminal relies on the satellite attitude control for pointing since it has no pointing capability (coarse or fine). The transmit laser divergence is 1 mrad; a 100-mW laser source is coupled with an EDFA for a total output power of 1 W [33]. Direct OOK modulation is applied to the laser source, up to 200 Mbps. OSIRIS V1 has launched in 2017 onboard the 110-kg Flying Laptop satellite in a 600-km sun-synchronous orbit with the goal of verification direct-to-art (DTE) optical communication. Laser pointing toward the ground station is carried out by the satellite bus. Attitude determination is given by two star-tracker and four fiber optical gyros, with total attitude knowledge of 7 arcseconds (≈ 0.1 mrad). Pointing accuracy is better than 100 arcsec (1.7 mrad). The terminal weighs 1.3 kg and consumes 26 W.

OSIRIS V2 [34] features the following improvements: data rate up to 1 Gbps with consequent reduction of transmit laser beamwidth divergence (≈ 0.2 mrad), dedicated InGaAs PIN quadrant detector for tracking the beacon laser sent by the ground station. The feedback given by this sensor is used by the satellite ADCS for closed-loop pointing of the ground station. The terminal weighs 1.65 kg and consumes up to 37 W. OSIRIS V2 was launched in 2016 onboard the Biros satellite.

OSIRIS V3 is the next installment and features increased data rate (up to 10 Gbps) and a coarse pointing assembly for independent beam steering, at the cost of the increased mass and power consumption (5 kg, 50 W). OSIRIS V3 is designed to operate onboard the ISS (launch scheduled in 2021).

OSIRIS4CubeSat, also known as CUBE LCT, is the smallest optical communication terminal available, developed by TESAT in collaboration with the Institute of Communications and Navigation of the German Aerospace Agency (DLR-IKN) [35]. The system is conceived for CubeSats. Volume, mass and power consumption are $90 \times 95 \times 35$ mm (0.3U), 397 g and 10 W.

It features a $\pm$ 1-degree fast steering mirror for fine pointing while coarse pointing is delegated to the host satellite bus. Telecom wavelength is 1550 nm. According to the producer, it can deliver 100 Mbps in downlink toward a 60-cm aperture ground telescope.

The first Cube LCT model was the payload of the 3U CubeSat PIXL-1, launched in January 2021 with the goal of demonstrating the transmission of high-resolution images via an optical channel. The OSIRIS terminals are shown in Fig. 15.7.

15.6.7 LEOCAT and CUBECAT

TNOs have been active in the last years in the development of optical communication terminal for small satellites [36].

LEOCAT is an optical head conceived for intersatellite connectivity. The unit has an envelope of $190 \times 190 \times 250$ mm, optical aperture of 70 mm and a FoV of ± 0.25 degree. The system features three optical channels (transmit, receive, and one dedicated to QKD) and a complex FPS, comprising one FSM for fine pointing of transmit and receive beam, another one for applying the point ahead angle to the transmit beam and a third one dedicated to the QKD beam. A CMOS camera is used for coarse acquisition and a quadrant detector for fine pointing through the FSMs. No CPS is conceived, nor there is information regarding the electronic subsystem. The LEOCAT prototype is shown in Fig. 15.8 (left).

CubeCat is a compact optical communication terminal for DTE applications fitting in one CubeSat unit. The system features an FPS based on an FSM, exploiting a 1590 nm beacon laser from the ground station, which is also used by the host satellite bus for coarse pointing. Uplink beacons can also carry information at 100 kbps. The 1545 transmit beam is OOK modulated at 1 Gbps. A rendered depiction of the system is shown in Fig. 15.8 (right).

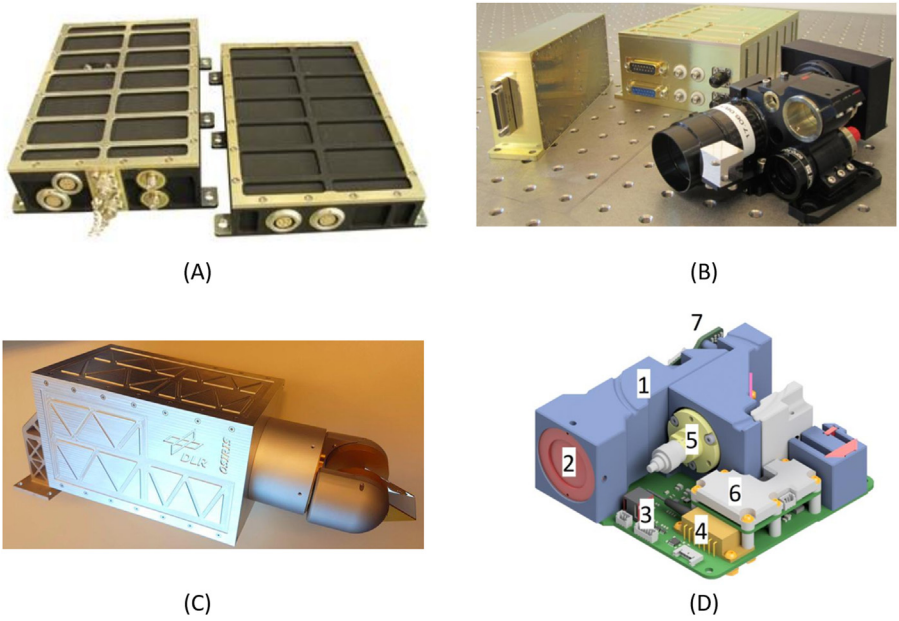

Figure 15.7 (A) Optical Space InfraRed downlInk System (OSIRIS) V1 [33], (B) OSIRIS V2 [34], (C) OSIRIS V3 mock-up [32], and (D) 3D model of Cube LCT [35], showing main components: (1) mechanical mounts, (2) optical elements, (3) electronics mainboard, (4) laser source, (5) the transmit collimator, (6) driver electronics with a passive cooling element, (7) receiver detector.

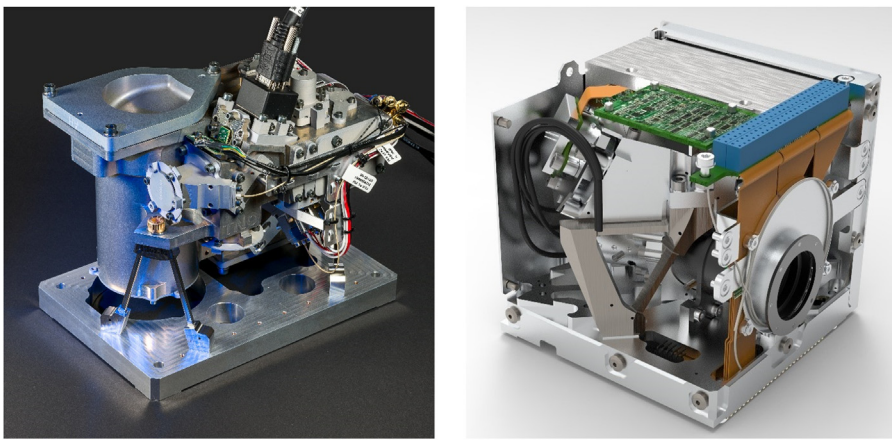

Figure 15.8 (Left) Render of LEOCAT telescope. (Right) Render of CUBECAT terminal. Both images from [37].

Table 15.4 Summary and comparison of optical terminals for small satellites.

Terminal	Mass [kg]	Power [W]	Volume [mm^3]	Optical aperture [mm]	Wavelength [nm]	Optical power [mW]	Bitrate [Mbps]	Pointing system
SOTA	5.7	39.5	177.5x117x278 (OPT) 146 × 160 × 110.5 (CONT)	50	980/1543	540/80	10	Coarse (gimbal) + fine
VSOTA	1	10	n.a.	n.a.	980/1543	540/80	0.1	fine
OCSD	n.a.	10−20	n.a.	n.a.	1064	2−4	100	fine
NODE	1.2	15	100 × 100 × 120	23	1550	0.2	50	fine
Fibertek LCT	2	20	100 × 100 × 200	64	1550	1−3	1000	fine
LaserCube	1.8	26	100 × 100 × 200 (DL) 100 × 100 × 220 (ISL)	42	1550	100 (DL) 450 (ISL)	1000 (DL) 200 (ISL)	Coarse + fine
OSIRIS V1	1.3	26	n.a.	n.a.	1550	1000	200	None
OSIRIS V2	1.65	37	n.a.	n.a.	1550	1000	1000	None
OSIRIS V3	5	50	n.a.	n.a.	1550	n.a.	10000	coarse
Cube LCT	0.4	10	90 × 95 × 35	18	1550	100	100	fine
LEOCAT	n.a.	n.a.	190 × 190 × 250	70	1550[a]	n.a.	n.a.	fine
CUBECAT	n.a.	n.a.	100 × 100 × 100	n.a.	1545	n.a.	1000	Fine

n.a., not available.
[a]Presumed.

15.6.8 Terminal comparison

A comparison of the main parameters of the laser communication terminals for small satellites presented in this chapter is presented in Table 15.4. Figs. 15.9 and 15.10 present the terminal's performance (bitrate) as a function of terminal mass and power consumption, respectively. Figs. 15.11 and 15.12 show the evolution of two performance parameters P_{kg} = Mbps/kg and P_W = Mbps/W. Some conclusions can be inferred from these data. First, it is clear that system efficiency has increased over the years, with both P_{kg} and P_W increasing. In addition, a significant effort has been put into miniaturization, starting from the 5.7 kg of SOTA to the very small size of VSOTA and Cube LCT. Finally, there seems to be an architectural trend

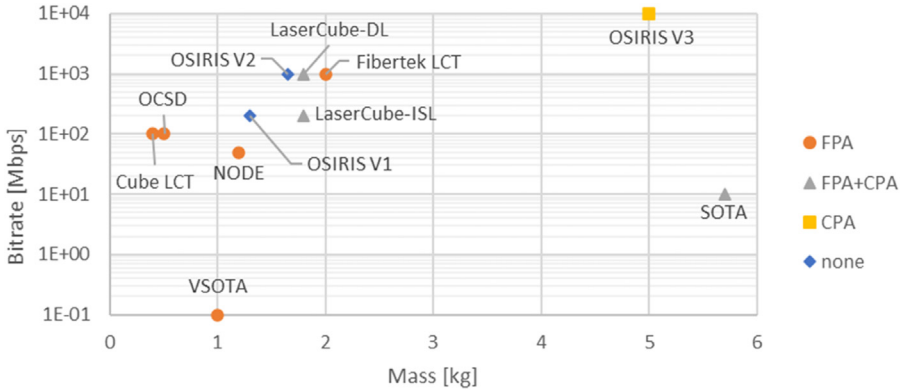

Figure 15.9 Bitrate versus mass for optical communication terminals for small satellites, grouped by type of pointing system.

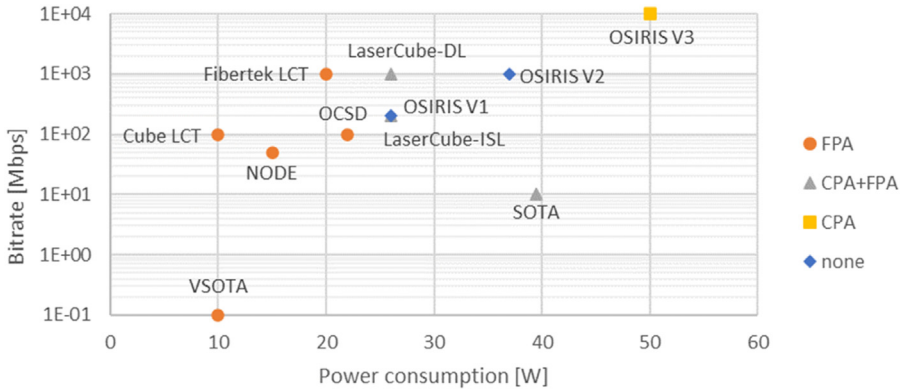

Figure 15.10 Bitrate versus power consumption for optical communication terminals for small satellites, grouped by type of pointing system.

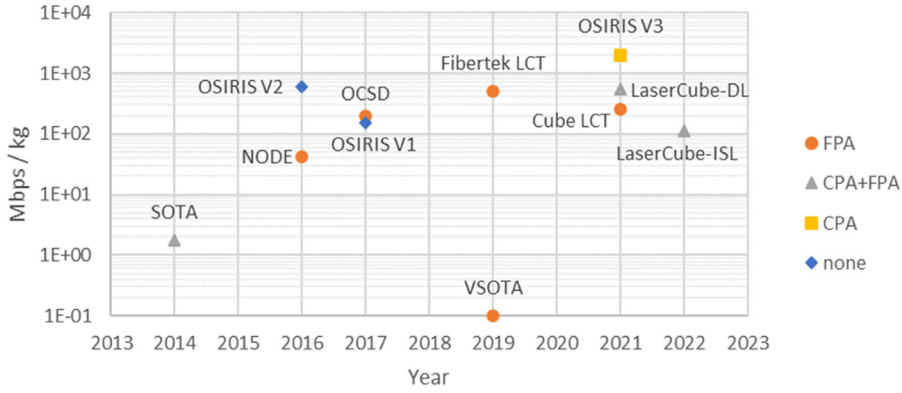

Figure 15.11 Trend of Mbps/kg for optical communication terminals for small satellites, grouped by type of pointing system.

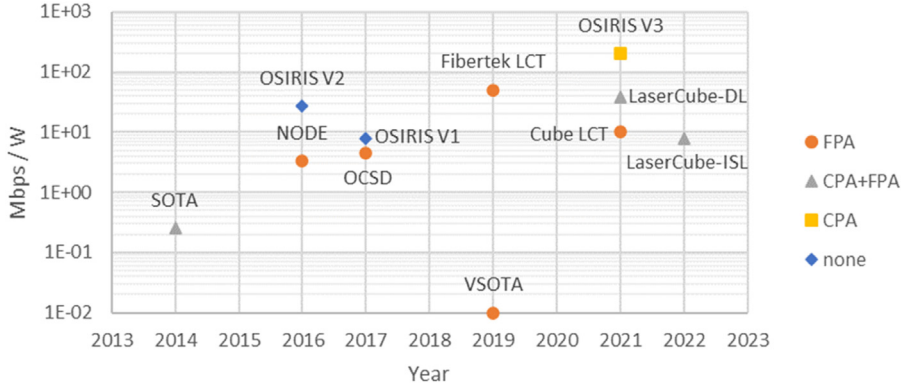

Figure 15.12 Trend of Mbps/W for optical communication terminals for small satellites, grouped by type of pointing system.

that penalizes the inclusion of a coarse pointing stage within the terminals, delegating this function to the host satellite ADCS. In fact, among the later terminals, only LaserCube and OSIRIS V3 feature a dedicated CPS.

15.7 Conclusions

Optical communication is an emerging technology that can revolutionize the telecommunication capabilities of small satellites. Thanks to the very narrow beams that can be obtained with compact aperture exploiting visible and near-infrared

wavelengths, high-data-rate point-to-point links can be realized in both direct-to-Earth and intersatellite links. The implementation of optical downlink and intersatellite links on LEO constellations based on small satellites may lead to the realization of advanced spaceborne networks with the capability to route and deliver to the end-users an unprecedented amount of data. The main applications benefitting from such advances will be Earth observation and the Internet of Things.

While optical communication has become a mature, yet not common technology for what concerns medium and large satellites, its exploitation in the field of small satellites is still in a pioneering phase. Several technologies and systems have been proposed recently, aiming at demonstrating the feasibility of optical communications with/between small satellites. The main challenges are represented by the pointing accuracy which is required to establish stable optical links, and the development of efficient laser sources and receiver electronics needed to cover long distances. For what concerns the pointing aspects, two main architectural solutions have been identified and pursued. On one hand, most proposed terminals feature some sort of fine-pointing stabilization of the transmit and receive beams, delegating the task of coarse pointing to the host satellite bus. While this represents a simplification in the development of the terminal, it poses severe requirements for the satellite ADCS. In fact, the limitations of small satellites, and in particular nanosatellites, attitude control capabilities often force to widen the transmit optical beam to limit pointing losses, partially losing the main benefit of optical communication (narrow beams, high directivity). On the other hand, providing the terminals with independent coarse pointing capability has the potential to improve the pointing accuracy, at the cost of increased terminal complexity, mass and power consumption.

Considering the optical communication terminals for small satellites developed in the last years, an evident trend toward miniaturization can be appreciated, being the latest systems dimensions compatible with CubeSat platforms. In general, performance parameters such as Mbps/W and Mbps/kg are increasing over time.

References

[1] K. Araki, Y. Arimoto, M. Shikatani, M. Toyoda, M. Toyoshima, T. Takahashi, Performance evaluation of laser communication equipment onboard the ETS-VI satellite, Proceedings of SPIE, Free-Space Laser Communication Technologies VIII (1996). San Jose.

[2] T. Tolker-Nielsen, J.C. Guillen, SILEX: the first European optical communication terminal in orbit, ESA Bulletin 96 (1) (1998) 998.

[3] Y. Fujiwara, et al., Optical inter-orbit communications engineering test satellite (OICETS), Acta Astronautica 61 (1-6) (2007) 163–175.

[4] R. Fields, C. Lunde, R. Wong, J. Wicker, D. Kozlowski, J. Jordan, et al., NFIRE-to-TerraSAR-X laser communication results: satellite pointing, disturbances, and other attributes consistent with successful performance, Proceedings of SPIE, Sensors and Systems for Space Applications III (2009).

[5] B.S. Robinson, et al. The NASA lunar laser communication demonstration—successful high-rate laser communications to and from the moon, in SpaceOps 2014 Conference, 2014.

[6] H. Takenaka, et al., Accuracy of satellite orbit prediction and optical design of optical ground station beacons for satellite-to-ground optical communication, International Conference on Space Optics—ICSO 2020 11852 (2021). International Society for Optics and Photonics.
[7] H. Henninger, H. Yamazoe, K. Iwamoto, First optical ground station integrated in a service provider network, Proc. 72nd International Astronautical Congress (IAC) 25−29 (2021). Dubai, United Arab Emirates.
[8] H. Kaushal, G. Kaddoum, Optical communication in space: challenges and mitigation techniques, IEEE Communications Surveys & Tutorials 19 (1) (2016) 57−96.
[9] H. Weichel, L. Beam, Propagation in the Atmosphere, SPIE, Bellingham, WA, 1990.
[10] B. Mayer, S. Shabdanov, D. Giggenbach, Electronic Data Base of Atmospheric Attenuation Coefficients (2002).
[11] D. Giggenbach, A. Shrestha, Atmospheric absorption and scattering impact on optical satellite-ground links, International Journal of Satellite Communications and Networking (2021).
[12] H. Kaushal, V. Kumar, A. Dutta, H. Aennam, H. Aennam, V. Jain, et al., Experimental study on beam wander under varying atmospheric turbulence conditions, IEEE Photonics and Technical Letters 23 (22) (2011) 1691−1693.
[13] L.C. Andrews, R.L. Phillips, C.Y. Hopen, Laser Beam Scintillation with Applications, SPIE Press, 2001.
[14] R. Rui-Zhong, Scintillation index of optical wave propagating in turbulent atmosphere, Chinese Phy. B 18 (2) (2009).
[15] L. Andrews, R. Phillips, Laser Beam Propagation through Random Media, 2nd ed., SPIE Press, 2005.
[16] C.E. Shannon, Communication in the presence of noise, Proceedings of the IRE 37 (1) (1949) 10−21.
[17] A. Bjarklev, D. Chowdhury, A. Majumdar, M. Nakazawa, C.G. Someda, H.G. Weber, Optical and fiber communications reports.
[18] A. Carrasco-Casado, et al., LEO-to-ground optical communications using SOTA (Small Optical TrAnsponder) − payload verification results and experiments on space quantum communications, Acta Astronautica 139 (2017) 377−384.
[19] H. Takenaka, et al. Satellite-to-ground quantum-limited communication using a 50-kg-class micro-satellite. Nature Photonics (August issue, 2017). http://www.nature.com/nphoton/index.html, https://doi.org/10.1038/nphoton.2017.107.
[20] Kubo-oka et al. Optical communication experiment using very small optical transponder component on a small satellite RISESAT, in Proceedings of the International Conference on Space Optical Systems and Applications (ICSOS) 2012, 11-4, Ajaccio, Corsica, France, October 9−12, 2012.
[21] Y. Koyama, et al., SOTA: Small Optical Transponder for micro-satellite, International Conference on Space Optical Systems and Applications (ICSOS). IEEE, 2011.
[22] T.S. Rose, et al., Optical communications downlink from a 1.5U CubeSat: OCSD program, Proc. International Conference on Space Optics—ICSO 2018 (2018). Chania, Greece, 9−12 October.
[23] S. Janson, et al. The NASA optical communications and sensor demonstration program - initial flight results, in 29th annual AIAA/USU Conference on Small Satellites, Logan, Utah, August 8−13, 2015.
[24] E. Clements, et al., Nanosatellite optical downlink experiment: design, simulation, and prototyping, Optical Engineering. 55 (11) (2016) 111610.

[25] C. Payne, et al. Integration and testing of the nanosatellite optical downlink experiment, in 32nd Annual AIAA/USU Conference on Small Satellites, Logan, Utah, August 4−9, 2018.
[26] Grenfell design and prototyping of a nanosatellite laser communications terminal for the Cubesat laser infrared crosslink (CLICK) B/C mission.
[27] B. Mathason, et al., CubeSat lasercom optical terminals for near-earth to deep space communications, Proceedings of the SPIE LASE (2019). San Francisco, California, United States.
[28] F. Sansone, et al., LaserCube optical communication terminal for nano and micro satellites, Acta Astronautica 173 (2020) 310−319.
[29] R. Antonello, et al. High precision dual−stage pointing mechanism for miniature satellite laser communication terminals, IEEE Transactions in Industrial Electronics.
[30] F. Sansone, F. Branz, A. Vettor, E. Birello, G. Paolo Guizzo, R. Antonello, A. Francesconi, Calibration and verification of pointing and tracking system for optical communication terminal, AIAA Journal 61 (2) (2023) 510−517.
[31] F. Sansone, et al., Towards in-orbit demonstration of a compact optical communications terminal for small satellites, Proceedings of the 71st International Astronautical Congress (IAC) − The CyberSpace Edition (2020). 12−14 October.
[32] C. Fuchs, C. Schmidt, Update on DLR's OSIRIS program, International Conference on Space Optics—ICSO 2018 11180 (2019). International Society for Optics and Photonics.
[33] D. Giggenbach, et al., Optical data downlinks from osiris on flying laptop satellite, Online Proceedings of TT&C 2019 (2019).
[34] C. Schmidt, et al., OSIRIS payload for DLR's BiROS satellite, International Conference on Space Optical Systems and Applications (2014) 2014.
[35] B. Rödiger, et al., High data-rate optical communication payload for CubeSats." Laser communication and propagation through the atmosphere and oceans IX. Vol. 11506, International Society for Optics and Photonics (2020).
[36] R. Saathof, et al., Optical satellite communication space terminal technology at TNO.", International Conference on Space Optics—ICSO 2018. 11180. International Society for Optics and Photonics (2019).
[37] R. Saathof, et al., In orbit demonstration plans for an optical satellite link between a CubeSat and a ground terminal at TNO, Free-Space Laser Communications XXXIII. Vol. 11678. SPIE, (2021).